STM observation of the hinge-states of bismuth nanocrystals

Tianzhen Zhang, Sergio Vlaic, Stéphane Pons, Dimitri Roditchev, Valeria Sheina, Christophe David, Guillemin Rodary, Jean-Christophe Girard, Hervé Aubin

STM observation of the hinge-states of bismuth nanocrystals

Tianzhen Zhang, Sergio Vlaic, Stéphane Pons, and Dimitri Roditchev
LPEM, ESPCI Paris, PSL Research University, CNRS, Sorbonne Université, 75005 Paris, France

Valeria Sheina, Christophe David, Guillemin Rodary, Jean-Christophe Girard, and Hervé Aubin
Universités Paris-Saclay, CNRS, Centre de Nanosciences et de Nanotechnologies, 91120, Palaiseau, France
(Dated: September 12, 2023)

The recent application of topological quantum chemistry to rhombohedral bismuth established the non-trivial band structure of this material. This is a 2^{nd}order topological insulator characterized by the presence of topology-imposed hinge-states. The spatial distribution of hinge-states and the possible presence of additional symmetry-protected surface-states is expected to depend on the crystal shape and symmetries. To explore this issue, we have grown bismuth nanocrystals in the tens of nanometers on the (110) surface of InAs. By scanning tunneling spectroscopy, we mapped the local density of states on all facets and identified the presence of the hinge-states at the intersection of all facets. Our study confirm the classification of bulk bismuth as a 2^{nd}order topological insulator. We propose that the ubiquitous presence of the hinge-states result from their tunnel-coupling across the nanometer-sized facets.

I. INTRODUCTION

Solids with filled electronic bands and no interactions may seem quite mundane, yet, band structures can have interesting non-trivial topological properties that can be inferred from their symmetries.

To analyse the symmetry properties of an atom located on a lattice site, it is usual to employ the representation theory [1] of point-groups to obtain the decomposition of the atomic orbitals as a direct sum of irreducible representations of the atomic site point-group symmetry.

By analogy, to analyse the symmetry properties of the Bloch states arising from these orbitals, band representations theory, a representation theory of space groups [2, 3], can be employed to obtain the decomposition of the band structure as a direct sum of irreducible band representations.

While band representation theory was barely used for decades, it have recently attracted intense interest with the demonstration that one band that cannot be decomposed into any linear combination of physical elementary band representation must have non-trivial topological properties. This gave birth to *topological quantum chemistry* [4] and enabled the identification and calculation of symmetry indicators for the 230 space groups [5–7], which are related to topological indexes, and facilitated large-scale search across databases to identify topological materials [8]. This has greatly expanded the topological classification of band insulators beyond the Z_2 topological insulators [9, 10] and revealed the existence of numerous symmetry-indicated topological phases such as mirror-symmetry-protected topological crystalline insulators (TCIs) [11, 12], rotational-symmetry–protected TCIs [13] and higher-order topological insulators (HOTIs) [14–18].

Although the lowest-symmetry HOTI models exhibit gapped two-dimensional surface-states and gapless one-dimensional hinge-states [5–7, 18], typical solid-state HOTIs have additional crystal symmetries that can protect gapless surface-states; thus, a HOTI can coexist with a TCI. Depending on the sample termination, the same crystal may exhibit either two-dimensional surface-states or gapped facets separated by topological hinge-states.

The application of topological quantum chemistry to rhombohedral bismuth (Bi), with space-group $R\bar{3}m$ (#166) and point-group D_{3d} has shown that its valence and conduction bands result from a split elementary band representation[17], which implies non-trivial topological properties. These topological properties result from a double band inversion [11, 19] at the same time-reversal-invariant momenta (TRIM) points. The topological phase can be described as two superposed copies of a TCI protected by time reversal T, threefold rotation $C_{3[111]}$ about the [111] direction and inversion I symmetries [17], characterized by the $Z_4 = 2$ topological index [5–7, 15, 18]. The fourfold Dirac surface-states of this topological phase are unstable[18, 20] and it has been shown that a crystal with an inversion-symmetric shape, such as a rod of hexagonal section oriented along the [111] direction, the mass of the Dirac states is of opposite sign on surfaces with inversion - related Miller indices, resulting in helical hinge modes encircling the crystal [17].

Experimentally, on hexagonal cavities in the (111) surface of *bulk* Bi [21], scanning tunneling microscopy (STM) and spectroscopy (STS) identified edge-states on every two edges of the cavity. Because two-dimensional bismuth was predicted theoretically to be a two-dimensional quantum spin Hall insulator (QSHI) with Kane-Mele index $Z_2 = 1$ [22, 23], the edge-states were identified with the topological states of a QSHI altered by the coupling to the bulk[21]. While later STM works indeed confirmed the presence of topological edge-states on thin bismuth films[24, 25] and bismuthene[26–28], those observed on *bulk* Bi cavities were later reinterpreted as the signature of the hinge-states of a HOTI[17]. Interestingly, the edge-states in bismuthene and hinge-states in Bi are related as it was shown that the stacking of multiple two-dimensional QSHI leads either to a

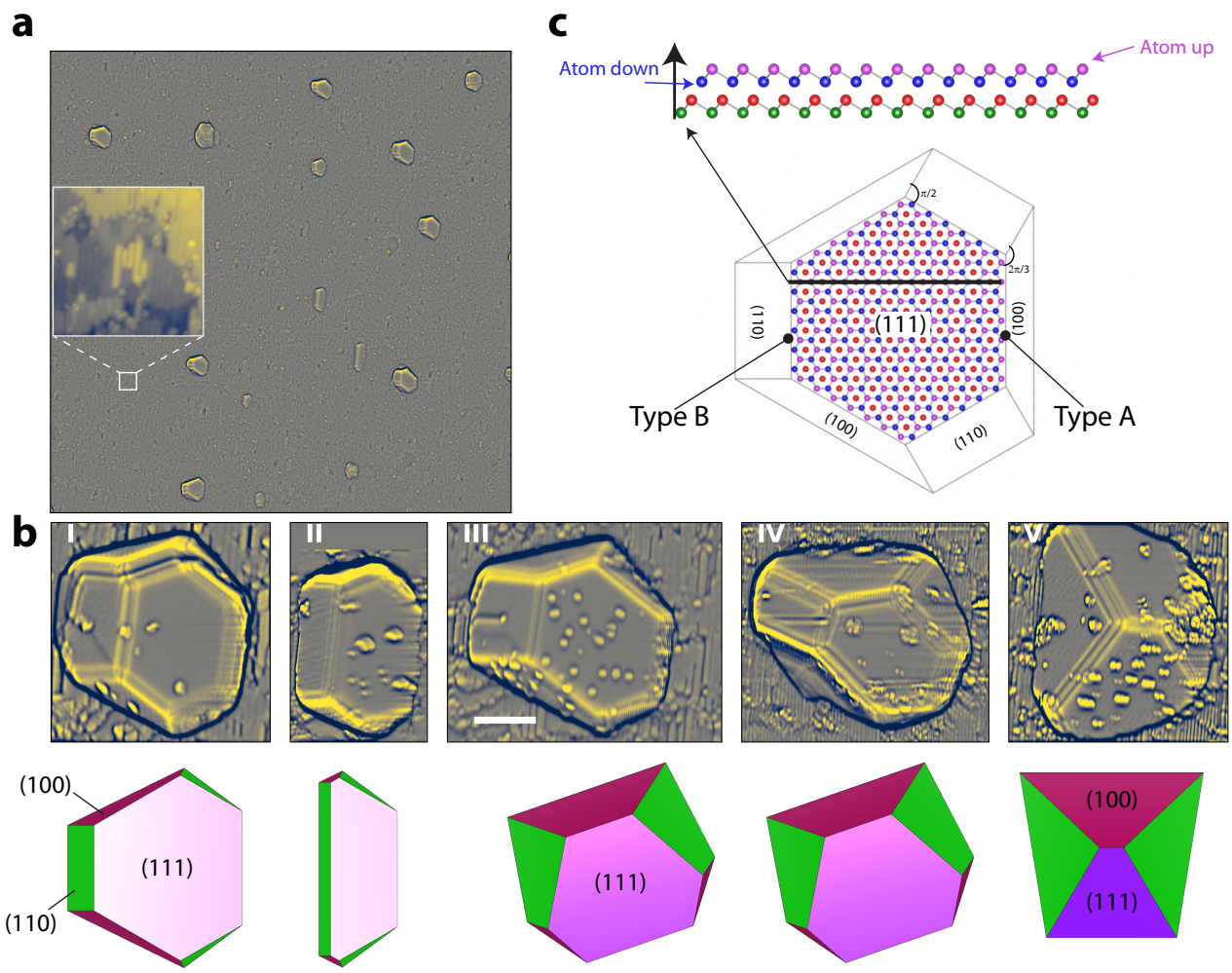

FIG. 1. (a) 800 nm × 800 nm Laplacian $\Delta_{xy}z(x,y)$ transform of a topographic STM image (I_{set} = 30 pA, V_{bias} = 1.5 V). The inset is a zoom on a zone 30 nm × 30 nm. (b) Laplacian $\Delta_{xy}z(x,y)$ transforms of selected topographic images, labelled from I to V. The scale bar on the third image is 10 nm long. Below each image, a model of the shape is provided where are indicated the Miller indices of the facets. (c) Top : Atomic model of two atomic bilayers of Bi. Bottom : Atomic model of a nanocrystal. The type B edge, last atom of the first bilayer pointing down, is located at the hinge between the (111) and (110) facets. The type A edge, last atom of the first bilayer pointing up, is located at the hinge between the (111) and (100) facets. As indicated, the edges of the (110) facet make an angle of $\pi/2$, the edges of the (100) facet make an angle of $2\pi/3$.

weak three-dimensional topological insulator or a HOTI. $Bi_{14}Rh_3I_9$ [29, 30] and Pt_2HgSe_{30} [31–34] are examples of the former; Bi[17], WTe_2[18] and Bi_4Br_4 [35] are examples of the latter. Finally, the presence of the hinge-states was also inferred from SQUID-like supercurrent oscillations observed with Josephson circuits fabricated on Bi[17, 36] and WTe_2 [37–39].

In addition to the HOTI phase protected by the $C_{3[111]}$ symmetry, it has been shown[40] that Bi is also host of a first-order TCI state protected by a twofold rotational symmetry $C_{2[1\bar{1}0]}$ about the $[1\bar{1}0]$ direction, resulting in a pair of topological Dirac surface-states on its $(1\bar{1}0)$ surface, coexsisting with the hinge-states of the HOTI phase. On (110) oriented Bi films, recent STM/STS measurements[41] have identified hinge-states that could be described by a HOTI protected by time-reversal symmetry and bulk two-fold rotation $C_{2[1\bar{1}0]}$[40]. The surface-states were not observed though, because of the broken translation symmetry on the $(1\bar{1}0)$ facets.

These recent theoretical and experimental works suggest that the distribution of surface- and hinge-states on a Bi crystal depends on its shape and transformation properties under $C_{3[111]}$, $C_{2[1\bar{1}0]}$ and inversion symmetries.

To explore the relationship between surface-states, hinge-states and the crystal shape, we have grown Bi nanocrystals on the (110) surface of InAs and characterized its electronic properties by STM/STS. Thanks to the small size of the nanocrystals and using very sharp STM-tips, we have been able to perform the STM/STS characterization of multiple facets and hinges of the nanocrys-

tals. We clearly identified hinge-states, confirming qualitatively the classification of Bi as a HOTI. However, we found that the spatial distribution of the density of states due to hinge-states could not be reproduced easily by a simple model with hinge-states appearing at the intersection of facets with Dirac masses of opposite signs[17, 40]. Instead we found hinge-states at the intersection of all facets, provided they are sufficiently extended. We suggest that the ubiquitous presence of hinge-states is the consequence of their hybridization due to tunnel-coupling across the nanometer-sized facets.

II. NANOCRYSTAL GROWTH

The Bi nanocrystals have been grown on the (110) surface of n-doped InAs, which substrate has been cleaved in ultra-high vacuum at base pressure P $\approx 10^{-10}$ mbar. The (110)-surface of InAs substrates has also been employed previously for the growth of superconducting Pb nanocrystals [42, 43] and Bi nanolines[44, 45]. By thermal evaporation, we deposited a nominal quantity of three monolayers of Bi at a temperature of 500 K. This is the optimum temperature for the growth of nanolines[45], where we checked their formation by low energy electron diffraction (LEED). A topographic STM image is shown in Fig. 1a, where Bi nanocrystals are visible as well as nanolines in the zoom insert. Consistently with past works on Bi nanolines [45], there is no indication of alloying with the InAs substrate. To accentuate the facets and edges, a Laplacian filter $\Delta_{xy} z(x, y)$ is applied to all topographic images. Fig. 1b show topographic images zoomed on five selected Bi nanocrysals, labelled I to V. The lateral size of nanocrystals is between 10 nm and 40 nm, the height is between 5 nm and 15 nm. To obtain such topographic images free from artifacts resulting from the shape of the tip, a tip-shaping procedure has been employed where the tip is approached into contact with the InAs surface, then, a large current of 1 μA is injected and the tip is slowly retracted. This tip-elongation procedure is repeated until no effects of the shape of the tip is visible on the topography of the nanocrystals. Using the crystallographic software VESTA[@] and employing the crystal structure of Bi, we model the shape of all nanocrystals and show the results below the corresponding nanocrystals in Fig. 1b. From these Wulf constructions, the crystallographic facets (111), (110) and (100) can be clearly identified for each nanocrystal. The (111) facet is the most stable surface of Bi [46] and can be clearly identified as the largest facet with hexagonal shape. This facet is surrounded by the (110) and (100) facets. The (110) facet has C_2 symmetry and its edges make an angle of $\pi/2$, the (100) facet has C_3 symmetry and its edges make an angle of $2\pi/3$. These two angles are indicated on Fig. 1c and allow the identification of the facets.

On the hexagonal cavity studied on the (111) surface of bulk Bi [21], two type of edges were identified with edge A (B) corresponding to the edge with last Bi atom pointing up (down). We use the same notation. As shown by the atomic model in Fig. 1c, the location of edges A and B can be identified on nanocrystals, which was not possible on the cavity. Edge A (B) is located at the intersection, i.e. hinge, between the (111) and the (100) ((110)) facets.

III. SCANNING TUNNELING SPECTROSCOPY

On these three-dimensional nanocrystals, it is possible to perform STS on multiple facets. We will now detail the results obtained on two selected nanocrystals. The results for nanocrystal I, which has large (111) and (110) facets, are shown in Fig. 2. The results for nanocrystal IV, which has large (111) and (100) facets, are shown in Fig. 3. Additional STS results for the nanocrystals II, III and V are shown in Fig. 4.

For all nanocrystals, a small Coulomb gap about 25 meV is visible at zero bias, as highlighted in Fig. 2c and Fig. 3c. As described in the previous work on Pb nanocrystals[42, 43], when a nanocrystal is grown atop a two-dimensional electron gas of Fermi wavelength larger than the nanocrystal lateral sizes, a quantum constriction effect occurs, similar to what observed in quantum-point contacts, reducing the transmission to values smaller than one quantum of conductance. In this situation, the nanocrystal is only weakly coupled to the substrate and so Coulomb blockade occurs. In our system, the Bi nanowires and nanocrystals have expected Fermi wavelengths in the 10 - 30 nm range [46], comparable to nanocrystals lateral sizes, explaining the observation of Coulomb blockade and implying that the Bi nanocrystals are only weakly coupled to the substrate.

Fig. 2c and Fig. 3c show the differential conductance (DC) $\frac{\mathrm{d}I}{\mathrm{d}V}(V)$ spectra measured on nanocrystal I and nanocrystal IV, respectively, at positions indicated by colors symbols on corresponding panels ab.

In the middle of the (111) facets (red hexagon symbols), the DCs present conductance peaks at V_{bias} = 0.23 V. This is a consequence of the saddle point in the higher-energy relation dispersion of (111) surface-states, identified in equations as high-energy surface-states (HESS)[46–48], shown in Fig. 2g, along the $\bar{\mathbf{\Gamma}} - \bar{\mathbf{M}}$ direction of the Brillouin zone shown in Fig. 2e. The corresponding energy range is indicated as green zones in Fig. 2cdgh and Fig. 3cd. The DCs also show a sharp increase near V_{bias} = -0.01 V, which is a consequence of the saddle point in the lower-energy relation dispersion of (111) surface-states, followed by a maxima about V_{bias} = -0.07 V, identified in equations as low-energy surface-states (LESS) where the corresponding energy range is indicated as blue zones in Fig. 2cdgh and Fig. 3cd.

On the edges of the (111) facets, the conductance peak at V_{bias} = 0.23 V due to high-energy surface-states is missing, instead, peaks in the DCs are observed at lower energy. For nanocrystal I, conductance peaks are ob-

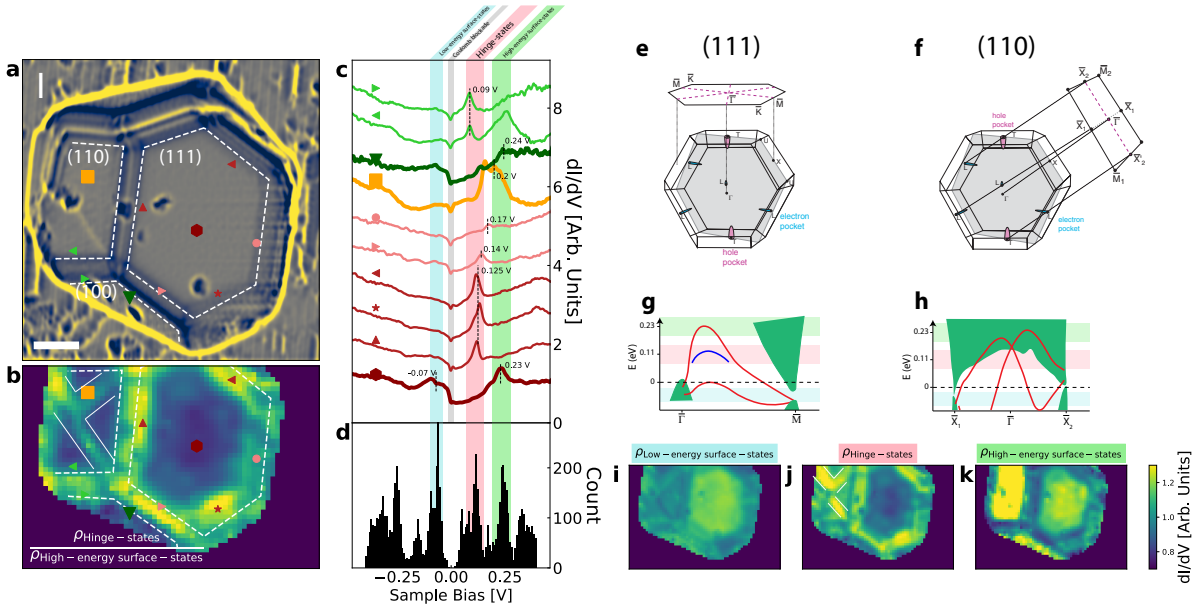

FIG. 2. STS data on nanocrystal I. (a) Laplacian $\Delta_{xy}z(x,y)$ transform of a topographic STM image (I_{set} = 30 pA, V_{bias} = 1.5 V). The scale bar is 5 nm long. The dashed lines indicate the edges between facets. (b) Conductance map $\frac{\rho_{HS}}{\rho_{HESS}}$ obtained by taking the ratio of the DC integrated on energy range of hinge-states, ρ_{HS}, with the DC integrated on energy range of high-energy surface-states, ρ_{HESS}. The scale is the same as panel (a). The dashed lines indicate the edges between facets. The white continuous lines indicate the diagonal-states generated by the defect in the middle of the (110) facet. Note how they merge with the hinge-states. (c) DC for selected points indicated as colored symbols on panels ab. The vertical colored rectangles indicate the energy ranges of interest corresponding, respectively, to low-energy surface-states, Coulomb gap, hinge-states and high-energy surface-states. The vertical dashed lines indicate conductance peaks of interest. See text. (d) Histogram of the energy values of conductance peaks identified in all DC curves measured on the nanocrystal. (e) Bulk Brillouin zone and pseudo-Brillouin zone of the (111) facet. (f) Bulk Brillouin zone and pseudo-Brillouin zone of the (110) facet. (g) Extracted from Ref. [46], the relations dispersions of projected bulk states (green areas), surface-states (red lines) and hinge-states (blue line) on the (111) facet. (h) Extracted from Ref. [46], the relations dispersions of projected bulk states (green areas) and surface-states (red lines) on the (110) facet. (i), (j) and (k) Conductance maps ρ_{LESS}, ρ_{HS} and ρ_{HESS} obtained by integrating the DCs on energy range of low-energy surface-states, hinge-states and high-energy surface-states, respectively.

served at V_{bias} = 0.125 V on all type-B edges (red symbols). On the two type-A edges measured (due to STM drift, the third one has not been measured), one large conductance peak is visible at V_{bias} = 0.14 V on the edge (pink right triangle) where the (100) facet is well defined but only a very small conductance peak (V_{bias} = 0.17 V) is visible on the second one (pink disk); we suggest this is due to the absence of the (100) facet for this edge where the (111) facet is reaching the InAs surface. For nanocrystal IV, on the type-B edges, the conductance peak at V_{bias} = 0.125 V is well defined only on the longest edge (red star symbol) but not on the two other short edges (red left- and up-triangles). On the type-A edges, the conductance peak at V_{bias} = 0.14 V is visible on two edges (pink right- and up-triangles), where the (100) facet is well defined, but not on the third one (pink disk symbol) where the (100) facet is absent and the (111) facet is reaching the InAs surface. As the symmetry arguments employed in topological quantum chemistry are very strong and do not depend on any particular model or adjustable parameters, the identification of these conductance peaks on both type of edges with the one-dimensional van Hove singularities of hinge-states expected for a second order topological insulator is one most reasonable assumption.

The hinge-states are labelled as HS in equations. Their energy range is indicated as pink zones in Fig. 2cdgh and Fig. 3cd. Thus, in contrast to the observation on cavities in the (111) surface of bulk Bi crystal[21], we find that the conductance peaks due to hinge-states are visible on both type of edges. As is also seen on the other nanocrystals, Fig. 4, the conductance peaks are visible only when the two facets making the hinge are extended and well defined.

In the middle of the (110) facet (orange square symbols), the DCs feature broad maxima at V_{bias} = 0.18 V, consistent with the observation of Ref. [41]. This maxima in the density of states is due to (110) surface-states[46, 49, 50], whose dispersion relation is shown Fig. 2h along the $\bar{\mathbf{X}}_1 - \bar{\mathbf{\Gamma}} - \bar{\mathbf{X}}_2$ direction of the Brillouin zone shown in Fig. 2f.

In the middle of the (100) facets (green down-triangle symbols), mostly visible in Fig. 3c of nanocrystal IV, the DCs feature broad maxima at V_{bias} = 0.24 V, which is

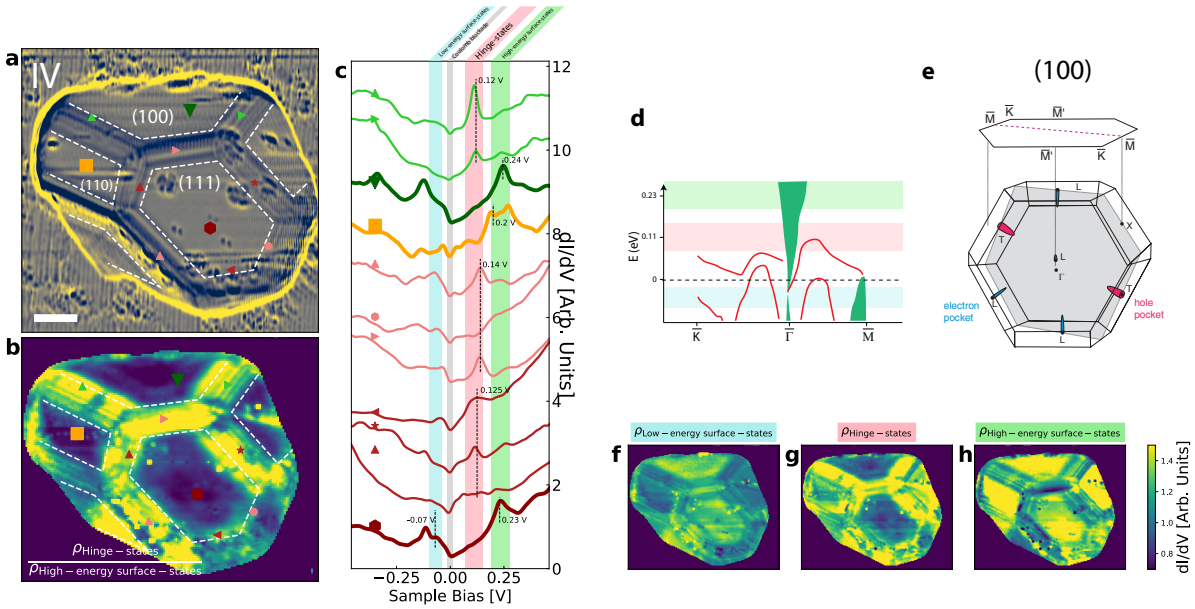

FIG. 3. STS data on nanocrystal IV. (a) Laplacian $\Delta_{xyz}(x,y)$ transform of a topographic STM image (I_{set} = 30 pA, V_{bias} = 1.5 V). The scale bar is 5 nm long. (b) Conductance map $\frac{\rho_{HS}}{\rho_{HESS}}$ obtained by taking the ratio of the DC integrated on energy range of hinge-states, ρ_{HS}, with the DC integrated on energy range of high-energy surface-states, ρ_{HESS}. The scale is the same as panel (a). (c) DC for selected points indicated as colored symbols on panels ab. The vertical colored rectangles indicate the energy ranges of interest corresponding, respectively, to low-energy surface-states, Coulomb gap, hinge-states and high-energy surface-states. The vertical dashed lines indicates conductance peaks of interest. See text. (d) Extracted from Ref. [46], the relations dispersions of projected bulk states (green areas), surface-states (red lines) and hinge-states (blue line) on the (100) facet. (e) Bulk Brillouin zone and pseudo-Brillouin zone of the (100) facet. (f), (g) and (h) Conductance maps ρ_{LESS}, ρ_{HS} and ρ_{HESS} obtained by integrating the DCs on energy range of low-energy surface-states, hinge-states and high-energy surface-states, respectively.

likely due to (111) surface-states[46].

Finally, on the hinges between the (110) and (100) facets (light green symbols), the DCs feature conductance peaks at $V_{bias} \approx 0.1$ V that indicates the presence of hinge-states. This is remarkable as they do not involve the (111) facet, which confirms the classification of Bi as a HOTI.

Two comments are in order.

First, we note that the energy of the van Hove singularities slightly changes from one hinge to the other; in particular, they have energies ≈ 0.125 eV for type-B edges and ≈ 0.14 eV for type-A edges. This change of energy could be explained by the hybridization between hinge-states located on opposite edges of the nanocrystal or because of different relation dispersions for the hinge-states on edges with different atomic terminations or arrangements.

Second, on all edges, the van Hove conductance peaks due to hinge-states appear concomitantly with the disappearance of the conductance peaks due to surface-states on all three facets. Such an anti-correlation was also observed previously[21].

To see this more clearly, we acquired full conductance maps, typically on a spatial grid of 64 pixels × 64 pixels and 512 voltage points. Fig. 2d shows an histogram of the energies of the conductance peaks identified in the 4096 DC spectra measured on the nanocrystal I. This histogram shows that the low-energy surface-states, high-energy surface-states and hinge-states are at the origin of all conductance peaks observed in the energy range [-0.25 eV, 0.25 eV]. There is no other major spectral feature of interest in this energy range on the whole nanocrystal.

To obtain maps of the local density of states, we remove the effects of changing tip-height and tunnel barrier energy by normalizing the DC spectra assuming that the total density of states is conserved on the energy range [-0.5 V, 0.5 V] measured. That is, the DC $\frac{dI}{dV}(V)$ spectra are normalized by their integrated values $\int_{-0.5}^{0.5} \frac{dI}{dV} dV$. Then, the normalized spectra are integrated on the three energy ranges corresponding to high-energy surface-states [0.19 V, 0.27 V], low-energy surface-states [-0.1 V, -0.04 V] and hinge-states [0.07 V, 0.15 V], to give ρ_{HESS}, ρ_{LESS} and ρ_{HS}, respectively, shown Fig. 2ijk and Fig. 3fgh for nanocrystal I and nanocrystal IV, respectively.

At the energy of high-energy surface-states, Fig. 2k and Fig. 3h, a large density of states is visible on all facets except on the edges. In contrast, at the energy of van Hove singularities due to hinge-states, Fig. 2j and Fig. 3g, a large density of states is observed on almost all hinges, between the (111) facet and (110), (100) facets as well as

between the (110) facets and the (100) facets. Note that a large density of hinge-states, is also observed in the middle of the largest (110) facet of nanocrystal I, surrounded by white continuous lines in Fig. 2j, seemingly as a consequence of the defect observed in the topography, Fig. 2a. Note also that the density of low-energy surface-states is mostly visible on the (111) and (100) facets and not on the (110) facets. Looking at the conductance maps Fig. 2jk and Fig. 3gh for both nanocrystal I and nanocrystal IV, respectively, the anti-correlation between the density of surface-states, ρ_{HESS}, and the density of hinge-states in the van Hove singularities, ρ_{HS}, is obvious. This suggests that a map of hinge-states can be obtained by calculating the ratio ρ_{HS}/ρ_{HESS}, which is shown Fig. 2b and Fig. 3b for both nanocrystal I and nanocrystal IV, respectively. In addition, Fig. 4 show the topography, ratio ρ_{HS}/ρ_{HESS} and DC spectra for the three additional nanocrystals : II, III and V.

For all nanocrystals, the map ρ_{HS}/ρ_{HESS} show that the topological states are clearly visible only at the hinges where two distinct Bi facets are well defined. See how the conductance peaks due to hinge-states disappear where the (111) facet reaches the InAs surface. This suggests that the hinge-states indeed arise from the interaction between surface-states as expected theoretically. More precisely, the theoretical model proposed in Ref. [17] implies the existence of two sets of surface-states resulting from two copies of the three-dimensional Z_2 topological insulator. The off-diagonal coupling between the two sets opens a gap for the surface-states, leaving only in-gap hinge-states at the edges of the facets. Thus, our STM/STS study of nanocrystals confirm the existence of hinge-states and so the classification of Bi as a HOTI.

To this topological interpretation, one could oppose a more trivial interpretation where the hinge-states result from chemical defects, such as dangling-bonds, at the facet edges. However, this interpretation is not consistent with the observation of hinge-states along the diagonals in the middle of (110) facets of nanocrystal I, Fig. 2b, nanocrystal III, Fig. 4e and nanocrystal V, Fig. 4h. For easy identification, they are surrounded by white continuous lines in those figure panels. While these diagonal-states seem to be the consequence from adatoms/defects in the middle of the (110) facet, as visible on the corresponding topographies, they are remarkable as they exist all along the diagonal of the (110) facets even where no defect is present. Furthermore, they are clearly seen to merge with the hinge-states on the edge with the (111) facet. This observation suggests that these diagonal-states are not related to local chemical defects, instead, they are related to the hinge-states and are circling around the nanocrystal as expected for topological hinge-states.

IV. DISCUSSION

Despite global consistency of the STS data with a HOTI model, there are two features that remain be understood theoretically. First, as mentioned above, the spectral weight associated with the hinge-states in the van Hove singularities appears concomitantly with the disappearance of the spectral weight associated with the high-energy surface-states. To highlight this anti-correlation between high-energy surface-states and hinge-states, Fig. 5efkl show the DC maps as function of sample voltage and distance along profiles drawn on the topographic images Fig. 5a(g) and ratio maps Fig. 5b(h) for nanocrystal I (IV). These maps show that the hinge-states appear at the expense of the surface-states on all facets. From the model of Ref. [17], we expect that the gap should remain constant on the whole surface of the nanocrystal, including the hinges; however, a redistribution of surface-states at the approach of the hinge can be expected but has not been discussed theoretically.

Second, according to this model applied to a rod of hexagonal section[17], the hinge-states should not exist on all hinges but only on those separating facets with Dirac masses of opposite signs. Instead, we observe topological states on all hinges except where the facet reaches the InAs substrate. We suggest that this ubiquitous presence result from the coupling between hinge-states on opposite sides of the facets. Indeed, it is well established that the tunnel coupling between the edge-states at opposite edges (surfaces) of a two-dimensional (three-dimensional) topological insulator leads to hybridization between edge states and to a gap opening in the relation dispersion of the edge-states Dirac spectrum [23, 27, 51–53]. This is also true for second-order topological insulator as shown recently for the corner-states of a two-dimensional second-order topological insulator [54]. In this last theoretical work, it has been shown that for well *localized* corner-states, the corresponding density of states is large on only some of the corners and not on others, however, when the wavefunctions of corner-states overlap, the corresponding density of states become equally distributed on all corners. As illustrated Fig. 6, in our small nanocrystals, significant overlaps of the wavefunctions describing the hinge-states located at opposite edges is to be expected, this could explain their presence on all hinges as well as the slightly different energy position of the van Hove singularities observed for different hinges due to gap opening in their relation dispersion. The possibility of a large coupling between hinge-states located at different edges is substantiated by a recent ab-initio study of Bismuth[55] indicating a deep penetration of the surface states within the bulk and that Bismuth should be considered bulk-like only for thickness larger than 400 nm.

While the effect of tunnel coupling between corner-states has been analyzed from tight-binding calculations on a two-dimensional lattice [54], the heavy computational cost for three-dimensional nanocrystals prevented

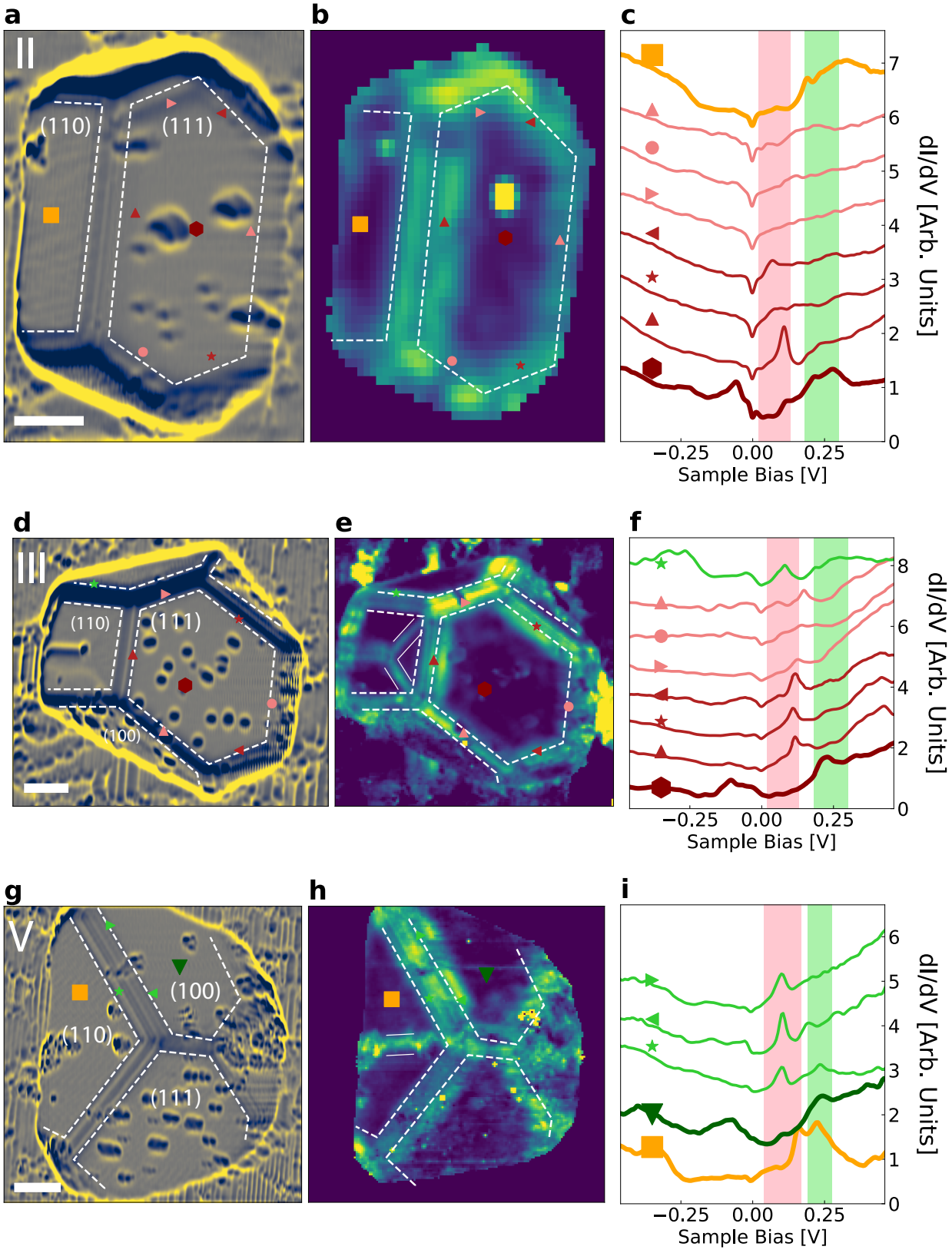

FIG. 4. (abc) STM/STS data for nanocrystal II. (a) Laplacian $\Delta_{xy}z(x,y)$ transform of a topographic STM image (I_{set} = 30 pA, V_{bias} = 1.5 V). The scale bar is 5 nm long. The dashed lines indicate the edges between facets. (b) Conductance map $\frac{\rho_{HS}}{\rho_{HESS}}$ obtained by taking the ratio of the DC integrated on energy range of hinge-states, ρ_{HS}, with the DC integrated on energy range of high-energy surface-states, ρ_{HESS}. The scale is the same as panel (a). The dashed lines indicate the edges between facets. (c) DC for selected points indicated as colored symbols on panels ab. The vertical colored rectangles indicate the energy ranges of interest corresponding, respectively, to the hinge-states and high-energy surface-states. (def) STM/STS data for nanocrystal III. (e) The continuous lines indicates the diagonal-states generated by the defect in the middle of the (110) facet visible on panel d. Note how they merge with the hinge-states. (ghi) STM/STS data for nanocrystal V.

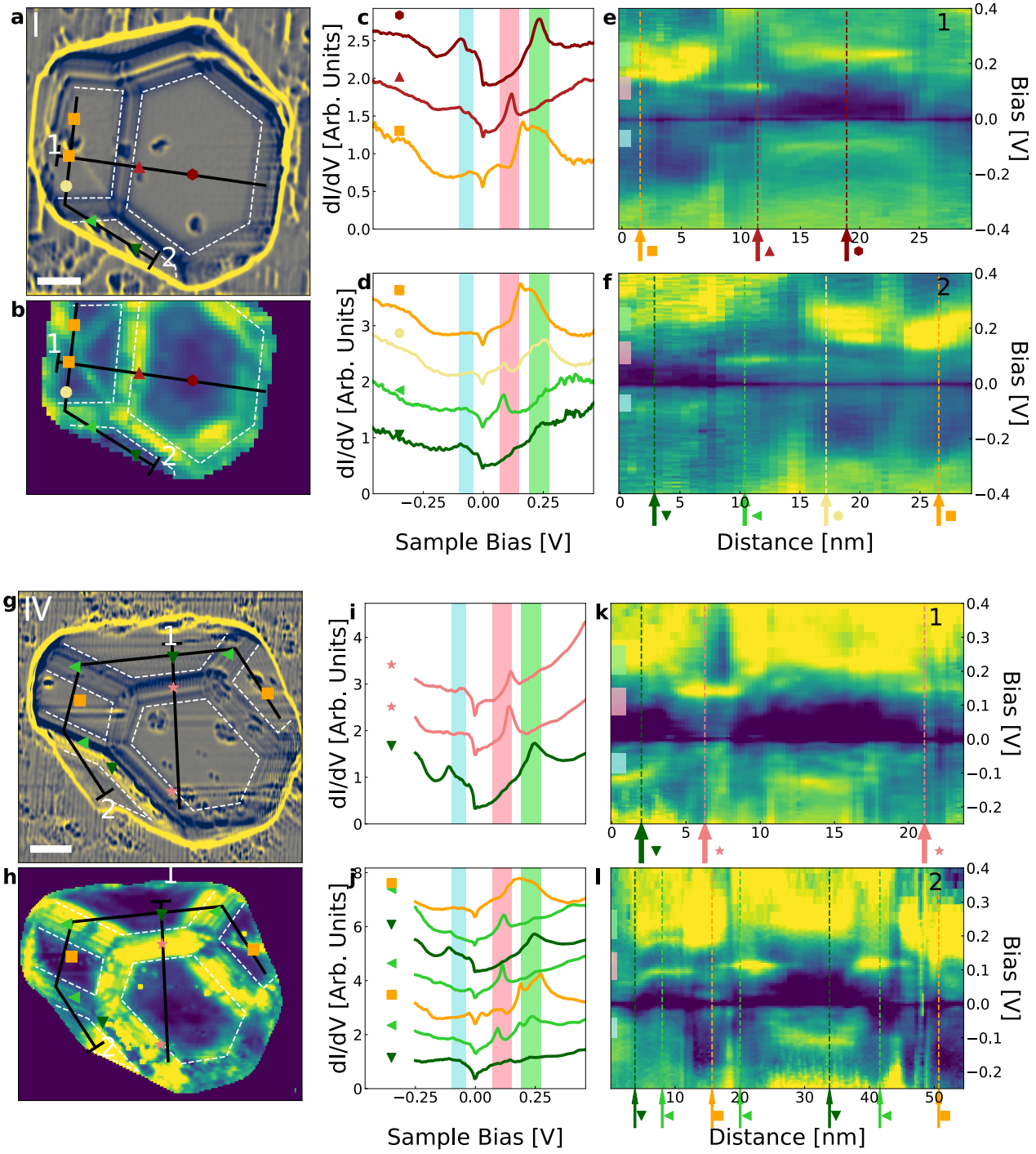

FIG. 5. STM/STS data for nanocrystal I. (a) Laplacian $\Delta_{xy}z(x,y)$ transform of a topographic STM image (I_{set} = 30 pA, V_{bias} = 1.5 V). The scale bar is 5 nm long. (b) Conductance map $\frac{\rho_{HS}}{\rho_{HESS}}$ obtained by taking the ratio of the DC integrated on energy range of hinge-states, ρ_{HS}, with the DC integrated on energy range of high-energy surface-states, ρ_{HESS}. The scale is the same as panel (a). (cd) DC for selected points indicated as colored symbols on panels ab and indicated as vertical dashed lines on panels ef. (ef) Conductance maps as function of sample bias and distance along the profiles drawn as black lines on panels ab. (ghijkl) STM/STS data for nanocrystal IV.

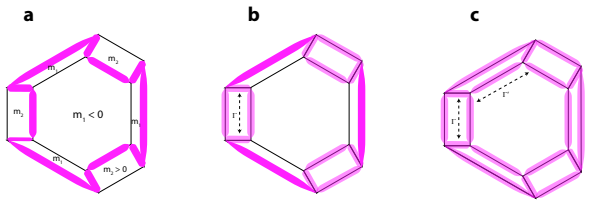

FIG. 6. Illustration of tunnel coupling between hinge-states. (a) In the absence of tunnel-coupling between opposite edges, the hinge-states encircle the nanocrystal following hinges where the gap (mass) changes sign between two facets, as described in Ref. [17]. (bc) In presence of tunnel-coupling Γ or Γ', the hinge-states become distributed on all edges.

us to perform such a tight-binding calculation. Furthermore, at hinges where several atomic steps exists, individual hinge-states separated in space by terraces should exist and for an even number of such states, they can hybridize and gap out. Note also that the observation of a van Hove singularity conductance peak does not imply that the hinge-state is topological. It is possible that only some of the hinge-states are gapless, while others are gapped, however, on the background of all the conducting states such a gap is difficult to observe by STM.

V. CONCLUSION

To summarize, we have shown that Bi nanocrystals could be grown on the (110) InAs surface. Their size in the tens of nanometer make them suitable for STM/STS studies on all facets of the tri-dimensional nanocrystal. We identified the hinge-states van Hove singularities at all hinges between the three facets (111), (110) and (100), however, on edges where the facet ends on the InAs substrate, no van Hove singularity is observed. These observations are consistent with the classification of Bi as a HOTI. We suggest that the ubiquitous observation of the van Hove singularities on all hinges result from their coupling across the nanometer sized facets. Further theoretical and numerical simulations are needed to confirm this suggestion.

ACKNOWLEDGMENTS

We acknowledge financial support from ANR MECHASPIN Grant No. ANR-17-CE24-0024-02 and ANR FRONTAL Grant No. ANR-19-CE09-0017-02. We thank S. Guéron, H. Bouchiat, T. Neupert and M. Denner for discussions, reading of the manuscript and suggestions.

[1] M. Tinkham, *Group Theory and Quantum Mechanics* (Dover Publications, 2003).
[2] J. Zak, Band representations of space groups, Phys. Rev. B Condens. Matter **26**, 3010 (1982).
[3] J. Cano, B. Bradlyn, Z. Wang, L. Elcoro, M. G. Vergniory, C. Felser, M. I. Aroyo, and B. A. Bernevig, Building blocks of topological quantum chemistry: Elementary band representations, Phys. Rev. B Condens. Matter **97**, 035139 (2018).
[4] B. Bradlyn, L. Elcoro, J. Cano, M. G. Vergniory, Z. Wang, C. Felser, M. I. Aroyo, and B. A. Bernevig, Topological quantum chemistry, Nature **547**, 298 (2017).
[5] H. C. Po, A. Vishwanath, and H. Watanabe, Symmetry-based indicators of band topology in the 230 space groups, Nat. Commun. **8**, 50 (2017).
[6] Z. Song, T. Zhang, Z. Fang, and C. Fang, Quantitative mappings between symmetry and topology in solids, Nat. Commun. **9**, 3530 (2018).
[7] E. Khalaf, H. C. Po, A. Vishwanath, and H. Watanabe, Symmetry indicators and anomalous surface states of topological crystalline insulators, Phys. Rev. X **8**, 031070 (2018).
[8] B. J. Wieder, B. Bradlyn, J. Cano, Z. Wang, M. G. Vergniory, L. Elcoro, A. A. Soluyanov, C. Felser, T. Neupert, N. Regnault, and B. A. Bernevig, Topological materials discovery from crystal symmetry, Nat. Rev. Mater. **7**, 196 (2021).
[9] M. Z. Hasan and C. L. Kane, Colloquium: Topological insulators, Rev. Mod. Phys. **82**, 3045 (2010).
[10] X.-L. Qi and S.-C. Zhang, Topological insulators and superconductors, Rev. Mod. Phys. **83**, 1057 (2011).
[11] J. C. Y. Teo, L. Fu, and C. L. Kane, Surface states and topological invariants in three-dimensional topological insulators: Application to Bi$_{-}$xSb$_x$, Phys. Rev. B Condens. Matter **78**, 045426 (2008).
[12] L. Fu, Topological crystalline insulators, Phys. Rev. Lett. **106**, 106802 (2011).
[13] C. Fang and L. Fu, New classes of topological crystalline insulators having surface rotation anomaly, Sci. Adv. **5**, eaat2374 (2019).
[14] Z. Song, Z. Fang, and C. Fang, (d-2)-dimensional edge states of rotation symmetry protected topological states, Phys. Rev. Lett. **119**, 246402 (2017).
[15] F. Schindler, A. M. Cook, M. G. Vergniory, Z. Wang, S. S. P. Parkin, B. Andrei Bernevig, and T. Neupert, Higher-order topological insulators, Sci. Adv. **4**, eaat0346 (2018).
[16] E. Khalaf, Higher-order topological insulators and superconductors protected by inversion symmetry, Phys. Rev. B Condens. Matter **97**, 205136 (2018).
[17] F. Schindler, Z. Wang, M. G. Vergniory, A. M. Cook, A. Murani, S. Sengupta, A. Y. Kasumov, R. Deblock, S. Jeon, I. Drozdov, H. Bouchiat, S. Guéron, A. Yazdani, B. A. Bernevig, and T. Neupert, Higher-Order topology in bismuth, Nat. Phys. **14**, 918 (2018).
[18] Z. Wang, B. J. Wieder, J. Li, B. Yan, and B. A. Bernevig, Higher-Order topology, monopole nodal lines, and the origin of large fermi arcs in transition metal dichalcogenides XTe$_{-}${2} (X=Mo,W), Phys. Rev. Lett. **123**, 186401 (2019).
[19] D. Hsieh, D. Qian, L. Wray, Y. Xia, Y. S. Hor, R. J. Cava, and M. Z. Hasan, A topological dirac insulator in

a quantum spin hall phase, Nature **452**, 970 (2008).
[20] B. J. Wieder, B. Bradlyn, Z. Wang, J. Cano, Y. Kim, H.-S. D. Kim, A. M. Rappe, C. L. Kane, and B. A. Bernevig, Wallpaper fermions and the nonsymmorphic dirac insulator, Science **361**, 246 (2018).
[21] I. K. Drozdov, A. Alexandradinata, S. Jeon, S. Nadj-Perge, H. Ji, R. J. Cava, B. Bernevig, and A. Yazdani, One-dimensional topological edge states of bismuth bilayers, Nat. Phys. (2014).
[22] S. Murakami, Quantum spin hall effect and enhanced magnetic response by spin-orbit coupling, Phys. Rev. Lett. **97**, 236805 (2006).
[23] M. Wada, S. Murakami, F. Freimuth, and G. Bihlmayer, Localized edge states in two-dimensional topological insulators: Ultrathin bi films, Phys. Rev. B: Condens. Matter Mater. Phys. **83**, 121310 (2011).
[24] L. Peng, J.-J. Xian, P. Tang, A. Rubio, S.-C. Zhang, W. Zhang, and Y.-S. Fu, Visualizing topological edge states of single and double bilayer bi supported on multibilayer bi(111) films, Phys. Rev. B Condens. Matter **98**, 245108 (2018).
[25] F. Yang, J. Jandke, T. Storbeck, T. Balashov, A. Aishwarya, and W. Wulfhekel, Edge states in mesoscopic bi islands on superconducting nb(110), Phys. Rev. B Condens. Matter **96**, 235413 (2017).
[26] F. Reis, G. Li, L. Dudy, M. Bauernfeind, S. Glass, W. Hanke, R. Thomale, J. Schäfer, and R. Claessen, Bismuthene on a SiC substrate: A candidate for a high-temperature quantum spin hall material, Science **357**, 287 (2017).
[27] R. Stühler, A. Kowalewski, F. Reis, D. Jungblut, F. Dominguez, B. Scharf, G. Li, J. Schäfer, E. M. Hankiewicz, and R. Claessen, Effective lifting of the topological protection of quantum spin hall edge states by edge coupling, Nat. Commun. **13**, 3480 (2022).
[28] S. Salehitaleghani, T. Maerkl, P. J. Kowalczyk, M. Le Ster, X. Wang, G. Bian, T.-C. Chiang, and S. A. Brown, Edge states of α-bismuthene nanostructures, 2D Mater. **10**, 015020 (2022).
[29] B. Rasche, A. Isaeva, M. Ruck, S. Borisenko, V. Zabolotnyy, B. Büchner, K. Koepernik, C. Ortix, M. Richter, and J. van den Brink, Stacked topological insulator built from bismuth-based graphene sheet analogues, Nat. Mater. **12**, 422 (2013).
[30] C. Pauly, B. Rasche, K. Koepernik, M. Liebmann, M. Pratzer, M. Richter, J. Kellner, M. Eschbach, B. Kaufmann, L. Plucinski, C. M. Schneider, M. Ruck, J. van den Brink, and M. Morgenstern, Subnanometre-wide electron channels protected by topology, Nat. Phys. **11**, 338 (2015).
[31] A. Marrazzo, M. Gibertini, D. Campi, N. Mounet, and N. Marzari, Prediction of a Large-Gap and switchable Kane-Mele quantum spin hall insulator, Phys. Rev. Lett. **120**, 117701 (2018).
[32] J. I. Facio, S. K. Das, Y. Zhang, K. Koepernik, J. van den Brink, and I. C. Fulga, Dual topology in jacutingaite Pt_2HgSe_3, Phys. Rev. Materials **3**, 074202 (2019).
[33] A. Marrazzo, N. Marzari, and M. Gibertini, Emergent dual topology in the three-dimensional Kane-Mele Pt_2HgSe_3, Phys. Rev. Research **2**, 012063(R) (2020).
[34] I. Cucchi, A. Marrazzo, E. Cappelli, S. Riccò, F. Y. Bruno, S. Lisi, M. Hoesch, T. K. Kim, C. Cacho, C. Besnard, E. Giannini, N. Marzari, M. Gibertini, F. Baumberger, and A. Tamai, Bulk and surface electronic structure of the Dual-Topology semimetal Pt_{2}HgSe_{3}, Phys. Rev. Lett. **124**, 106402 (2020).
[35] R. Noguchi, M. Kobayashi, Z. Jiang, K. Kuroda, T. Takahashi, Z. Xu, D. Lee, M. Hirayama, M. Ochi, T. Shirasawa, P. Zhang, C. Lin, C. Bareille, S. Sakuragi, H. Tanaka, S. Kunisada, K. Kurokawa, K. Yaji, A. Harasawa, V. Kandyba, A. Giampietri, A. Barinov, T. K. Kim, C. Cacho, M. Hashimoto, D. Lu, S. Shin, R. Arita, K. Lai, T. Sasagawa, and T. Kondo, Evidence for a higher-order topological insulator in a three-dimensional material built from van der waals stacking of bismuth-halide chains, Nat. Mater. **20**, 473 (2021).
[36] A. Bernard, Y. Peng, A. Kasumov, R. Deblock, M. Ferrier, F. Fortuna, V. T. Volkov, Y. A. Kasumov, Y. Oreg, F. von Oppen, H. Bouchiat, and S. Guéron, Long-lived andreev states as evidence for protected hinge modes in a bismuth nanoring josephson junction, Nat. Phys. **19**, 358 (2023).
[37] Y.-B. Choi, Y. Xie, C.-Z. Chen, J. Park, S.-B. Song, J. Yoon, B. J. Kim, T. Taniguchi, K. Watanabe, J. Kim, K. C. Fong, M. N. Ali, K. T. Law, and G.-H. Lee, Evidence of higher-order topology in multilayer WTe2 from josephson coupling through anisotropic hinge states, Nat. Mater. **19**, 974 (2020).
[38] A. Kononov, G. Abulizi, K. Qu, J. Yan, D. Mandrus, K. Watanabe, T. Taniguchi, and C. Schönenberger, One-Dimensional edge transport in Few-Layer WTe2, Nano Lett. **20**, 4228 (2020).
[39] C. Huang, A. Narayan, E. Zhang, X. Xie, L. Ai, S. Liu, C. Yi, Y. Shi, S. Sanvito, and F. Xiu, Edge superconductivity in multilayer WTe2 josephson junction, Natl. Sci. Rev. **7**, 1468 (2020).
[40] C.-H. Hsu, X. Zhou, T.-R. Chang, Q. Ma, N. Gedik, A. Bansil, S.-Y. Xu, H. Lin, and L. Fu, Topology on a new facet of bismuth, Proc. Natl. Acad. Sci. U. S. A. **116**, 13255 (2019).
[41] L. Aggarwal, P. Zhu, T. L. Hughes, and V. Madhavan, Evidence for higher order topology in bi and Bi0.92Sb0.08, Nat. Commun. **12**, 4420 (2021).
[42] S. Vlaic, S. Pons, T. Zhang, A. Assouline, A. Zimmers, C. David, G. Rodary, J.-C. Girard, D. Roditchev, and H. Aubin, Superconducting parity effect across the anderson limit, Nat. Commun. **8**, 14549 (2017).
[43] T. Zhang, S. Vlaic, S. Pons, A. Assouline, A. Zimmers, D. Roditchev, H. Aubin, G. Allan, C. Delerue, C. David, G. Rodary, and J.-C. Girard, Quantum confinement effects in pb nanocrystals grown on InAs, Phys. Rev. B Condens. Matter **97**, 214514 (2018).
[44] W. G. Schmidt, Adsorption of group-v elements on III–V (1 1 0) surfaces, Surf. Sci. Rep. **25**, 141 (1996).
[45] M. G. Betti, D. Berselli, C. Mariani, N. Jedrecy, M. Sauvage-Simkin, Y. Garreau, and R. Pinchaux, (1 × 2) bi chain reconstruction on the InAs(110) surface, Phys. Rev. B: Condens. Matter Mater. Phys. **59**, 15760 (1999).
[46] P. Hofmann, The surfaces of bismuth: Structural and electronic properties, Prog. Surf. Sci. **81**, 191 (2006).
[47] Y. M. Koroteev, G. Bihlmayer, J. E. Gayone, E. V. Chulkov, S. Blügel, P. M. Echenique, and P. Hofmann, Strong Spin-Orbit splitting on bi surfaces, Phys. Rev. Lett. **93**, 046403 (2004).
[48] Y. M. Koroteev, G. Bihlmayer, E. V. Chulkov, and S. Blügel, First-principles investigation of structural and electronic properties of ultrathin bi films, Phys. Rev. B

Condens. Matter **77**, 045428 (2008).
[49] A. Takayama, T. Sato, S. Souma, and T. Takahashi, Rashba effect in antimony and bismuth studied by spin-resolved ARPES, New J. Phys. **16**, 055004 (2014).
[50] A. Takayama, T. Sato, S. Souma, T. Oguchi, and T. Takahashi, One-dimensional edge states with giant spin splitting in a bismuth thin film, Phys. Rev. Lett. **114**, 066402 (2015).
[51] B. Zhou, H.-Z. Lu, R.-L. Chu, S.-Q. Shen, and Q. Niu, Finite size effects on helical edge states in a quantum spin-hall system, Phys. Rev. Lett. **101**, 246807 (2008).
[52] Y. Zhang, K. He, C.-Z. Chang, C.-L. Song, L.-L. Wang, X. Chen, J.-F. Jia, Z. Fang, X. Dai, W.-Y. Shan, S.-Q. Shen, Q. Niu, X.-L. Qi, S.-C. Zhang, X.-C. Ma, and Q.-K. Xue, Crossover of the three-dimensional topological insulator Bi2Se3 to the two-dimensional limit, Nat. Phys. **6**, 584 (2010).
[53] J. Jung, A. Odobesko, R. Boshuis, A. Szczerbakow, T. Story, and M. Bode, Systematic investigation of the coupling between One-Dimensional edge states of a topological crystalline insulator, Phys. Rev. Lett. **126**, 236402 (2021).
[54] N. Arai and S. Murakami, Anisotropic penetration depths of corner states in a Higher-Order topological insulator, J. Phys. Soc. Jpn. **90**, 074711 (2021).
[55] I. Aguilera, H.-J. Kim, C. Friedrich, G. Bihlmayer, and S. Blügel, Z_2 topology of bismuth, Phys. Rev. Materials **5**, L091201 (2021).